PAPER

Mitigation of MHD induced fast-ion redistribution in MAST and implications for MAST-Upgrade design

To cite this article: D.L. Keeling *et al* 2015 *Nucl. Fusion* **55** 013021

IOP Publishing | International Atomic Energy Agency Nuclear Fusion
Nucl. Fusion **55** (2015) 013021 (16pp) doi:10.1088/0029-5515/55/1/013021

Mitigation of MHD induced fast-ion redistribution in MAST and implications for MAST-Upgrade design

D.L. Keeling[1], T.R. Barrett[1], M. Cecconello[2], C.D. Challis[1], N. Hawkes[1], O.M. Jones[1,3], I. Klimek[2], K.G. McClements[1], A. Meakins[1], J. Milnes[1], M. Turnyanskiy[4] and the MAST Team[1]

[1] CCFE, Culham Science Centre, Abingdon, Oxon., OX14 3DB, UK
[2] Department of Physics and Astronomy, Uppsala University, SE-751 05 Uppsala, Sweden
[3] Department of Physics, Durham University, South Road, Durham DH1 3LE, UK
[4] ITER Physics Department, EFDA CSU Garching, Boltzmannstraße 2, D-85748 Garching, Germany

E-mail: David.Keeling@ccfe.ac.uk

Received 7 July 2014, revised 2 October 2014
Accepted for publication 23 October 2014
Published 19 December 2014

Abstract

The phenomenon of the redistribution of neutral beam fast ions due to magnetohydrodynamic (MHD) activity in plasma has been observed on many tokamaks and more recently has been a focus of research on MAST (Turnyanskiy *et al* 2013 *Nucl. Fusion* **53** 053016). $n = 1$ fishbone modes are observed to cause a large decrease in the neutron emission rate indicating the existence of a significant perturbation of the fast-ion population in the plasma. Theoretical work on fishbone modes states that the fast-ion distribution itself acts as the source of free energy driving the modes that cause the redistribution. Therefore a series of experiments have been carried out on MAST to investigate a range of plasma densities at two neutral-beam power levels to determine the region within this parameter space in which fishbone activity and consequent fast-ion redistribution is suppressed. Analysis of these experiments shows complete suppression of fishbone activity at high densities with increasing activity and fast-ion redistribution at lower densities and higher neutral-beam power, accompanied by strong evidence that the redistribution effect primarily affects a specific region in the plasma core with a weaker effect over a wider region of the plasma. The results also indicate the existence of correlations between gradients in the modelled fast-ion distribution function, the amplitude and growth rate of the fishbone modes, and the magnitude of the redistribution effect. The same analysis has been carried out on models of MAST-Upgrade baseline plasma scenarios to determine whether significant fast-ion redistribution due to fishbone modes is likely to occur in that device. A simple change to the neutral-beam injector geometry is proposed which is shown to have a significant mitigating effect in terms of the fishbone mode drive and is therefore expected to allow effective plasma heating and current drive over a wider range of plasma conditions in MAST-Upgrade.

Keywords: neutral-beam injection, MAST, MHD, fast ions

(Some figures may appear in colour only in the online journal)

1. Introduction

The neutral-beam injection (NBI) system on MAST consists of two injection devices capable of injecting neutral deuterium with energies up to 75 keV and total power exceeding 2 MW per injector [1]. NBI has been used extensively in recent MAST experimental campaigns to access high performance operational regimes relevant to the operational domain of MAST-Upgrade [2, 3], which is currently under construction.

Efficient plasma core heating relies on good confinement of the NBI fast ions (FIs) so it is important to understand the transport mechanisms affecting FIs in order to design and access high performance and advanced plasma scenarios. Collisional diffusion of FIs is well understood [4] however, increasingly, anomalous transport processes are being recognized as a significant factor and is the motivation behind the present work. In this work a study is executed that examines in detail the redistribution of the FI population within and loss of FIs from the plasma due to particular magnetohydrodynamic (MHD) activity. In so doing, an operational domain is identified in which these redistribution and loss mechanisms are minimized and operation of the machine up to its full potential can be realized.

The phenomenon of core MHD affecting the FI distribution in tokamaks has been known since the early 1980s [5] and has been observed and studied in more detail recently in MAST [6]. In MAST plasma heated by NBI, neutron emission is dominated by interaction of the beam FIs with the background thermal plasma ions. Detailed observation of the neutron emission may therefore be used as a proxy measurement for the high-energy part of the spectrum of the NBI FI distribution (above ∼40 keV) within the plasma. In the previous study [6], a drop in the neutron emission rate correlated with MHD activity was observed as NB FIs were expelled from the plasma or redistributed into regions in which the reaction rate was lower. It was further observed that reducing the NBI heating power or changing the geometry of the NBI, such that NBI FIs were injected at an off-axis location, could reduce the FI redistribution effect. It was suggested that this reduction in redistribution was due to reduction of the FI pressure gradient. This inspired the present work to characterize the domain where such redistribution could be avoided and develop a means to extrapolate this to MAST-Upgrade.

2. Diagnostics and modelling

MAST plasmas have typical parameters of $R \sim 0.85$ m, $a \sim 0.65$ m, $I_p < 1$ MA, $B_t < 0.58$ T (where I_p is total plasma current and B_t is the toroidal field) and the device is equipped with a comprehensive set of high quality diagnostics enabling detailed modelling of the thermal plasma and FI population. Included in the suite of plasma diagnostics are three devices which give complementary measurements that may be used to determine FI behaviour in MAST; these are depicted in figure 1. Firstly, a uranium fission chamber (FC) [7] provides measurements of the total volume-integrated neutron emission rate. The FC is absolutely calibrated with time resolution of 10 μs. Secondly, a radially scanning neutron camera (NC) [8] simultaneously views four chords through the plasma, two on the machine midplane with different tangency radii separated by 20 cm and two angled downwards such that their tangency points are 20 cm below the midplane with the same horizontal separation as the midplane chords, note that only the midplane chords are used in this investigation. The position of the NC (i.e. the tangency radius of the line of sight of the viewing chord, labelled R_T in figure 1) may be changed between shots to achieve viewing chords with different tangency radii in the range $0\,\text{m} < R_T < 1.21\,\text{m}$ (positional accuracy of ± 3 cm), covering the core region of the plasma and beyond. This scanning capability, combined with the excellent repeatability of MAST plasmas, may be used to deduce profiles of neutron emissivity via forward modelling with fine spatial resolution. Each of the four channels measures spatially collimated line-integrated 2.5 MeV neutron flux from the plasma within each camera channel's field-of-view with a typical time resolution of 1 ms. Due to the finite acceptance angle of each chord, accurate modelling of the camera geometry is necessary to enable quantitative interpretation of the NC data.

Finally, a fast-ion D-alpha (FIDA) system [9] provides further information about the FI population. The FIDA diagnostic detects Balmer-alpha light from charge exchange of FIs with beam neutrals. The FIDA camera may be set in either

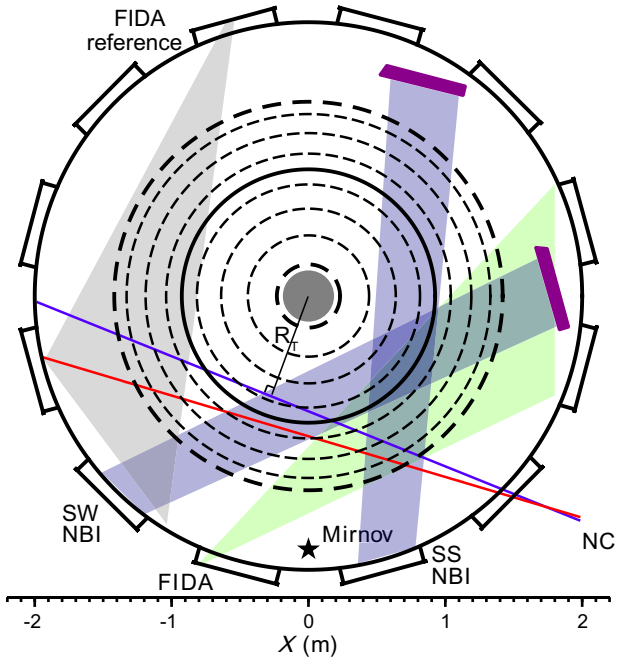

Figure 1. An equatorial cross-section of MAST showing the geometry of the FI diagnostics referred to in this study. Vacuum vessel (black), supercusp (SS) and chequerboard (SW) NBI footprints (shaded blue areas) and beam dumps (dark magenta), NC lines of sight (red and blue lines, tangency radius indicated as R_T), FIDA tangential active and reference fields of view (light green and grey shaded area), Mirnov coil (black star) and typical magnetic flux surfaces (dashed lines) with magnetic axis (solid line).

of two viewing configurations. The first is a near-toroidal view from a lens assembly mounted just above the vessel midplane with lines of sight intersecting the path of one of the neutral beams at major radii from 0.77 to 1.43 m. The second view is near-vertical looking down onto the path of the neutral beam. Eleven lines of sight are available which may be any mixture of toroidal or vertical views and passive lines of sight with similar viewing geometries, but which do not intersect the neutral beams, provide background subtraction of bremsstrahlung and passive FIDA light (i.e. FIDA emission from edge neutrals). The near-toroidal views are sensitive to high-energy passing FIs ($E > 44$ keV), providing complementary measurements to the neutron emission diagnostics since neutrons are produced primarily from interactions of the high-energy FIs. Note that only data from the near-toroidal views are used in the present work.

The complete suite of high spatial and temporal resolution diagnostics on MAST allows accurate interpretive analysis to be carried out. These include a 160 point, 200 Hz Thomson scattering (TS) system [10] providing measurements of plasma electron temperature and density. Edge neutral atomic density and edge density gradients are provided by an absolutely calibrated linear D-alpha camera [11, 12]. Charge-exchange recombination spectroscopy provides measurements of ion temperature and plasma rotation profiles. A 2D visible bremsstrahlung imaging camera [13], combined with the TS data, provides Z-effective measurements. A motional Stark effect (MSE) diagnostic [14] provides a measure of the pitch angle of the magnetic field and can be used in conjunction with the EFIT++ code [15] to determine the plasma current profile.

Together, these measurements provide a basis for interpretive modelling of the plasma.

For this study the interpretive code of choice is TRANSP [16]. TRANSP includes the NUBEAM Monte Carlo (MC) neutral beam code [17] which calculates the beam particle deposition profile and tracks the fast-particle guiding centres to thermalization or loss from the plasma. To improve accuracy NUBEAM employs a Larmor orbit correction. In this approach at each time step and for each MC particle, a 'random' gyro-phase is selected then a Newton–Raphson search algorithm is used to find the position of a particle point in real space that corresponds to that guiding centre. The plasma parameters local to this position, rather than at the position of the guiding centre, are then used in the collision operator. The effect over many poloidal orbits and a sufficiently large MC population is to create a distribution function that is close to that which would be created by a full gyro-orbit calculation. The EFIT++ code is employed using magnetic, kinetic and MSE constraints to provide plasma equilibria. A pre-processor code suite is used to self-consistently prepare the input data for the TRANSP simulations ensuring accurate mapping of necessary data to the EFIT++-derived plasma equilibria.

The two neutral-beam injectors installed on MAST during the recent experimental campaign have identical geometry: horizontal injection at the machine midplane with tangency radius = 70 cm. The injectors themselves were identical except for the configuration of the ion sources. Ion sources on NB injectors produce a low-density, low-temperature plasma from which ions are extracted and accelerated to create the energetic particle beam [18, 19]. Neutrals with different energies are eventually created depending on the molecular composition and charge states that exist in the source plasma (principally D^+, D_2^+, D_3^+). Depending on the detailed configuration of the confining magnetic field on the ion source, the various charge species can be enhanced or suppressed with respect to one another. On one beamline the source was in a so-called 'supercusp' configuration which enhances production of full-energy (D^+) component ions. On the other beamline the source was in a so-called 'chequerboard' configuration which enhances production of half- and third-energy component ions. The different configurations (the names of which refer to the geometry of the magnetic filter on the ion source) were in use to assess their relative merits with a view to selecting one or the other as most beneficial for the forthcoming MAST-Upgrade. This results in the beams having different ratios of Full : Half : Third energy neutral components. For the results presented in this study the 'supercusp' source provides power fractions in the ratio 0.89 : 0.08 : 0.03 and the 'chequerboard' source in the ratio 0.56 : 0.27 : 0.17. This is not a problem in the analysis since the species mix is taken into account by the NUBEAM code.

The calculated total neutron emission rate from TRANSP may be compared with the global neutron emission rate as measured by the fission chamber diagnostic. TRANSP is also able to output the full FI distribution function $f\left(R, Z, E, v_{||}/v\right)$ (R,Z = spatial coordinates, E = particle energy, $v_{||}/v$ = pitch angle cosine with respect to the magnetic field, assumes toroidal rotational symmetry) as well as the neutron emission mapped on a 2D poloidal cross-section at arbitrary times in the simulation. This data can then be processed with the LINE2 code [20] to produce profiles of the neutron emission rate as measured by the scanning NC. Thus measurements from two independent diagnostics may be compared with state-of-the-art interpretive modelling of experimental data. This combination allows robust conclusions to be drawn concerning the evolution of the FI population.

3. Experiments

3.1. Experimental basis and design

The growth rate (γ) of the mode causing fishbone (FB) instabilities is related to gradients in the 6D FI distribution function (f_{FI}) by [21, 22]

$$\gamma \propto \omega \frac{\partial f_{\mathrm{FI}}}{\partial E} - n \frac{\partial f_{\mathrm{FI}}}{\partial P_\varphi} \tag{1}$$

where ω is the mode frequency, E is fast particle energy and $P_\varphi = mRv_\varphi - e\psi$ (where m is the particle mass, R is the major radius, v_φ is the toroidal velocity and ψ is the poloidal flux function) is the canonical toroidal angular momentum. Using the approximation $P_\varphi = -e\psi$, P_φ can be thought of as a negative radial co-ordinate so the second term in equation (1) effectively becomes a radial gradient in the FI distribution function, $\partial f/\partial \psi_{\mathrm{p}}$. This relation implies that a negative energy gradient in the FI distribution function will decrease the growth rate of the FB mode whereas a negative radial gradient provides a source of free energy to drive the mode growth rate. In this experiment, the injection energy is kept constant so there should be little variation in the energy gradient between experiments. Changing the plasma density and/or the input power, however, should produce significant modification of the radial gradient of the distribution function. Increasing the power at constant injection energy increases number of particles deposited at a particular location in the plasma approximately in proportion to the increase in power, assuming constant plasma density. This increase in magnitude of the FI population will increase the magnitude of the radial gradient (which is negative since the FI population tends to be peaked at the plasma magnetic axis) and increase the mode growth rate. At higher plasma density, the FI distribution is still centrally peaked though the peaking factor is somewhat reduced due to the aforementioned changes in the NBI particle deposition profile. A decrease of the plasma density allows deeper penetration of the beam into the plasma core and cause proportionally greater deposition of beam particles in the core. At lower density, an increase in plasma electron temperature for a given heating power will also be expected which will increase the slowing down time of the FIs. These effects will both act to increase the FI pressure and hence increase the radial gradient of the FI distribution function.

The experiments carried out were therefore designed to explore a range of plasma density and NBI power levels in a plasma scenario that was operationally relevant to MAST-Upgrade. The intention of the experiment was to map out boundaries of the operational domain that could be accessed with low amplitude FB instabilities such that significant redistribution of NB FIs is suppressed. The scan in density naturally refers to the plasma electron density since this is the

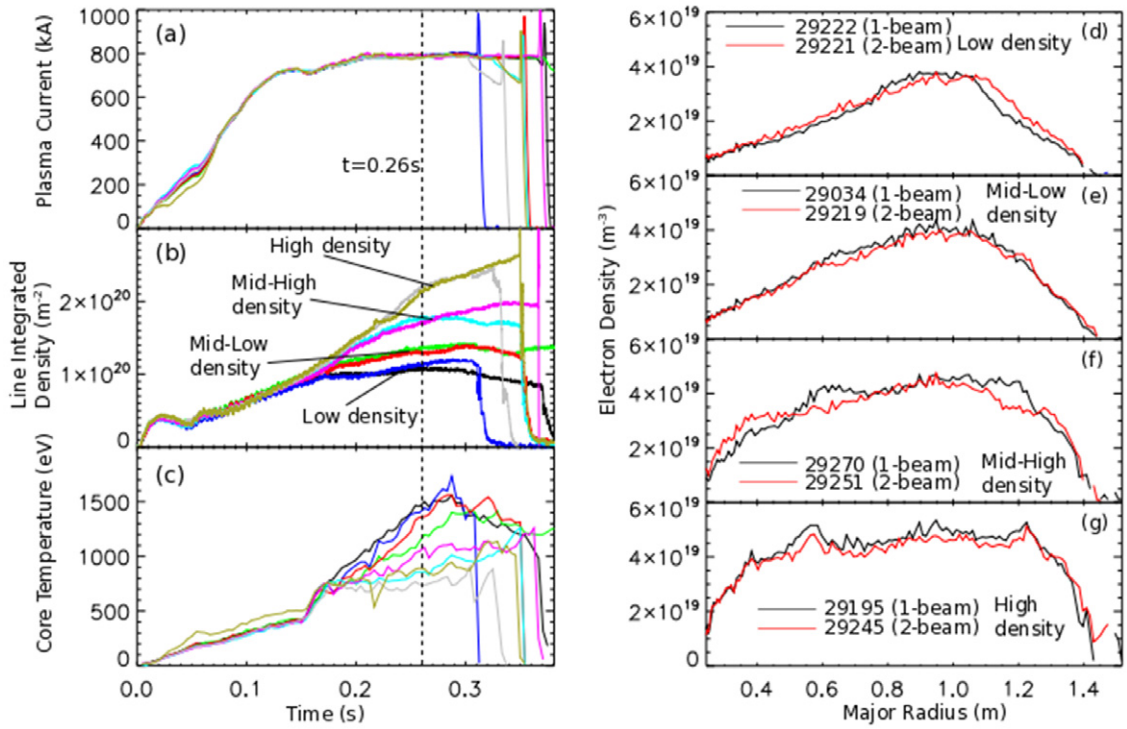

Figure 2. Time traces of (*a*) plasma current, (*b*) interferometer measurements of line-integrated electron density and (*c*) TS measurements of core electron temperature for the eight shots comprising the power/density scan. (*d*)–(*g*) TS electron density profiles taken at $t = 0.26$ s of the one-beam (black) and two-beam (red) shots at each density level.

quantity measured by a real-time Michelson interferometer diagnostic though plasma ion density is also measured by charge-exchange recombination spectroscopy and is included in the subsequent interpretive analysis. In referring to the scan in the subsequent discussion, the term 'plasma density' is used for brevity but is understood to refer to the measured plasma electron density. The shot sequence carried out to explore the density/power parameter space comprised a four-point scan in plasma density with two shots at each density level with one- and two-beam heating respectively, providing scans of density at two constant NBI power levels or viewed the other way, scans of NBI power at four constant plasma density levels. Other plasma parameters such as position, shape, NBI energy and NB start time were kept as identical as possible shot-to-shot. In the one-beam shots, the same beam (that fitted with the 'supercusp' ion source) was used. At the injection energy chosen (60 keV), the injected neutral power from this beamline was 1.5 MW. Care was taken to obtain the same injection energy on each beamline ensuring that the full, half and third energy components had the same birth energies and steps in the energy spectrum were as close as possible to that present in the one-beam shots. At the injection energy chosen, the neutral power injected by the second beamline (that fitted with the 'chequerboard' source) was 1.6 MW. Of course, considering the different ion sources in use on the two beamlines a small perturbation to the energy gradient is expected but this was assumed to be small compared to the changes effected in $\partial f/\partial \psi_p$. MSE measurements may only be obtained when the 'supercusp' beam is injecting power hence the choice of this for the single beam shots resulting in MSE measurements being available for all eight shots in the parameter scan. At the highest and lowest plasma density levels, the single beam shots were repeated a number of times with the scanning NC in a different position during each shot. This allowed the reconstruction of the neutron emission profile at the extremes of the plasma density scan allowing further conclusions to be drawn concerning the spatial extent of the phenomena being studied.

The principal features of the plasma scenario used for this study were: a 'direct-induction' start-up technique producing an 800 kA flat-top plasma current (see figure 2(*a*)), 0.585 T toroidal field and neutral beams starting at 150 ms (one- or two-beam depending on the particular shot). The 'direct induction' start-up was developed in the previous MAST experimental campaign to be as relevant as possible to MAST-Upgrade. The poloidal field coil set in MAST-Upgrade will not be compatible with merging compression, in which plasma is initiated around in-vessel poloidal field coils. Instead, 'direct induction' forms the plasma in the machine midplane and the use of this technique in the present study ensured that the early evolution of plasma temperature, density and current profile was as close as possible to that expected in MAST-Upgrade. Figure 2(*b*) shows the time evolution of the line-integrated electron density for each of the eight shots studied. In the period of interest, between 250–270 ms, these resulted in line-averaged electron density levels of between 2.0 and $4.5 \times 10^{19}\,\mathrm{m}^{-3}$. The radial profiles of the electron density as measured by the TS diagnostic at 260 ms are shown in figures 2(*d*)–(*g*) demonstrating very similar electron density profiles for the one-beam and two-beam shots at each of the four plasma density levels in the scan.

At the electron temperatures typically reached in MAST (typically 800 eV $< T_e <$ 1500 eV) fusion-neutron

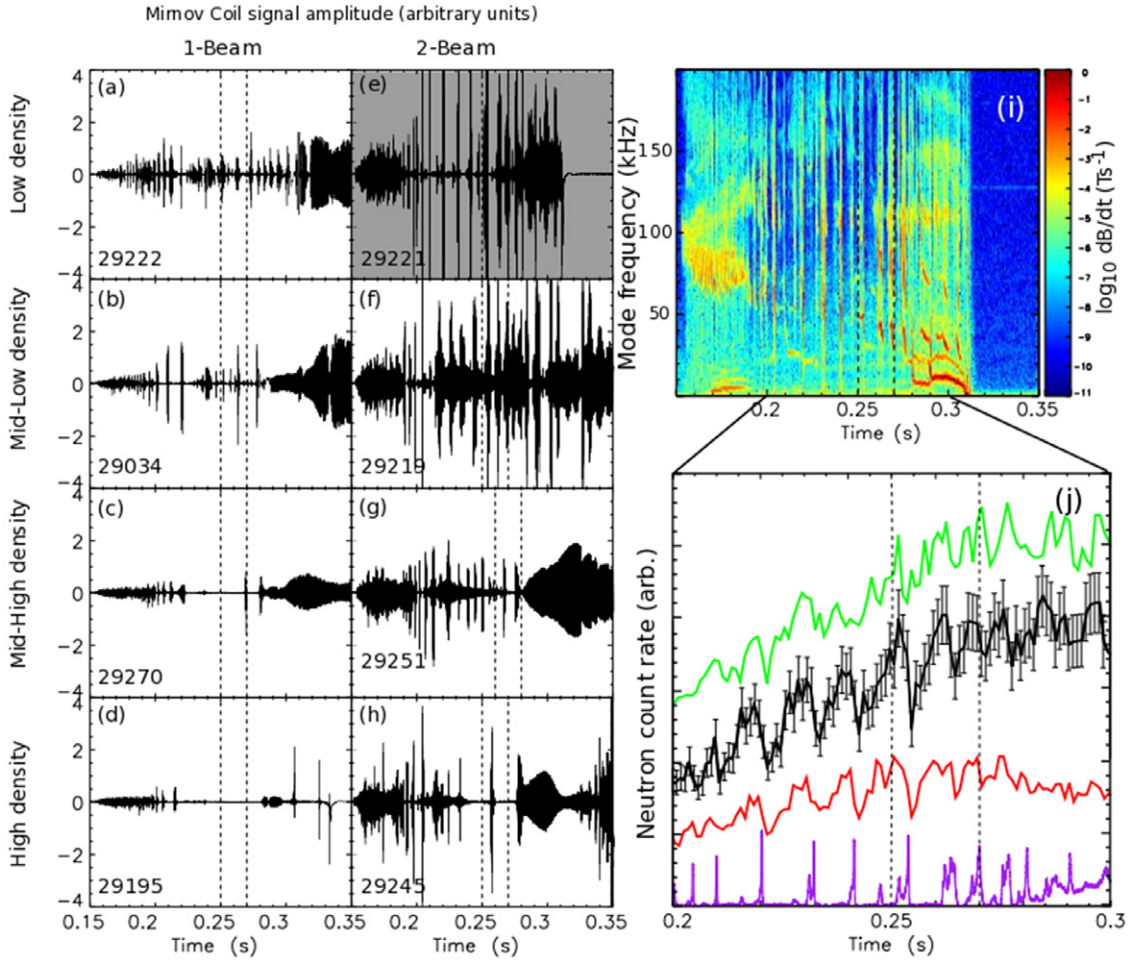

Figure 3. (*a*)–(*h*) Time traces from a Mirnov coil situated on the outboard side of MAST for the density/power scan with the POI for each shot marked by vertical dashed lines. (*i*) Magnetics spectrogram of shot 29221 (low density, two-beam indicated in grey in figure 2(*e*)) illustrating the presence of $n = 1$ FB modes during the POI (0.25–0.27 s, indicated). (*j*) Neutron emission rates for shot 29221; green: fission chamber measurement, black: NC midplane inboard chord ($R_T = 0.95 \pm 0.03$ m), red: NC midplane outboard chord ($R_T = 1.14 \pm 0.03$ m), purple: rms of Mirnov coil signal. Drops in neutron emission rate are very well correlated with FB modes, particularly in the NC signals. Error bars indicating a 10% relative error are shown for one of the NC chords [24] which are of a similar magnitude to errors in the FC signal (8.5% relative magnitude, omitted for clarity).

production is dominated by beam–thermal and beam–beam interactions which account for >99% of the total emission. Thermonuclear reactions contribute a negligible proportion of the total (<<1%). This makes the neutron emission profile a useful diagnostic tool to track changes in the FI distribution and any observed drops in the neutron emission rate can be interpreted as a reduction of the FI reaction rate in the region of the plasma under observation. In the absence of any other changes to plasma parameters, this can in turn be interpreted as a loss of FIs from that region or, in the case of a global measurement, a redistribution of the FIs into regions with lower thermal ion temperature where the steady-state reaction rate will be reduced [23] and/or ejection of FIs from the plasma.

Figure 3 details the MHD activity from the eight shots comprising the power/density scan and shows, for one representative shot, the correlation between the FB activity and abrupt changes in the neutron emission rate. Figures 3(*a*)–(*h*) show time traces obtained using a Mirnov coil mounted on the low-field side (LFS) of the vessel (LFS-MC) for the eight shots in the power/density scan. It is obvious from simple inspection of these time traces that higher NBI power at constant plasma density or lower plasma density at constant NBI power leads to higher amplitude MHD modes. Figure 3(*i*) shows the spectrogram of the low-density two-beam shot (29221, figure 3(*e*)) representing the case with the highest amplitude MHD activity. The 'chirping' modes that are of particular interest in this investigation (i.e. which 'chirp' down in frequency from about 50 kHz to about 20 kHz) are seen to occur from about 220 ms onwards in this shot. These 'chirping' modes during the period-of-interest (POI) are identified as $n = 1$ FB modes [6] where n is the toroidal mode number. Figure 3(*j*) shows the neutron emission rate from the low plasma density two-beam shot obtained using the fission chamber (black) and the two midplane chords of the scanning NC (green and red). The purple line shows the root-mean-square (rms) amplitude of the Mirnov coil signal. Simple inspection of these signals shows that the abrupt drops in neutron emission rate measurements are well-correlated with the FB modes. The high plasma density one-beam

shot representing the case with completely suppressed MHD activity (shot 29195) has also been used as the reference case in [24] in which results are presented concerning the modelling of different perturbations to classical FI simulations and their comparison with NC measurements.

From the spectrogram (figure 3(*i*)), it is clear that the beam-on period can be broadly divided into three distinct phases. In the early phase from beam-on at 150 ms to around 220–250 ms broadband toroidal Alfvén eigenmodes are apparent with a frequency in the range 50–100 kHz. Next, from 250 to around 280–300 ms, there is a phase which contains principally FB modes each chirping down in the frequency range from 50–20 kHz corresponding to orbital frequencies of nearly trapped passing FIs. In the high plasma density one-beam case, this phase is MHD free. From 280–300 ms, the so-called long-lived mode (LLM), associated with the existence of a $q = 1$ surface in the plasma, appears and continues to the end of the shot. These phases occur at similar times in all eight shots in the parameter scan as the q-profile evolves throughout each shot. In MAST-Upgrade it is desirable to develop an operational scenario with q just above 1 in the core of the plasma to avoid the LLM (which can be seen in the MHD spectrogram for MAST shot 29221 in figure 3(*i*) starting at ∼290 ms). It is therefore the phase with the core FB modes that is of interest as the plasma in this phase, particularly the form of the q-profile, most closely resembles that expected to be favourable for such stationary operation of MAST-Upgrade. Analysis has therefore focussed on a short interval just before the appearance of the LLM and is referred to as the POI. This is the period 250–270 ms for all the shots with one exception. In shot 29251 (medium–high plasma density, two beams), a large amplitude low-frequency mode (identified as a neoclassical tearing mode) is apparent that starts at around 200 ms and survives to 260 ms. Since the presence of this mode may also influence the FI distribution and is not specifically the type of MHD activity that is of interest, the POI for this shot is taken as 260–280 ms. Some residual effect of the low-frequency mode can be expected during the period 260–280 ms but, since the MHD activity during this period appears to be very similar to that observed in the other shots, i.e. it consists of FB modes, and the appearance of the LLM occurs after 280 ms, the period 260–280 ms for this shot is considered more representative of the effect of the FB modes. The POI is indicated by vertical dashed lines in all panels of figure 3. Defining these POIs allows time averages of various quantities to be taken during a well-defined period for each shot, illustrating the effect FB modes on the FI population.

3.2. Comparison of results with modelling

As discussed in section 2, the TRANSP code was used in conjunction with the high quality data available from the MAST diagnostics to produce interpretive simulations of the eight shots in the power/density scan. A figure of merit that can be examined to assess the quality of a TRANSP run is the calculated total neutron emission rate as compared to the total neutron emission rate measured by the fission chamber. Of course, for most of these shots, the neutron emission rate is not a good measure as this is strongly affected by the observed FBs. Hence examination of the calculated and measured neutron emission rates for the high plasma density one-beam case (shot 29195, figure 4(*a*) (inset)) shows that, in the absence of FBs, the neutron emission rate calculated by TRANSP is in excellent agreement with the rate measured by the FC. Furthermore, a detailed sensitivity study by Klimek and co-workers [24] has also shown that typical uncertainties in the experimental data used in the interpretive modelling result in much smaller uncertainties in the neutron emission rate than the changes observed during FB activity. It is concluded therefore that such changes are not related to experimental errors in the neutron measurements but rather arise from genuine effects of FBs on the FI population.

From the TRANSP simulations, it is possible to obtain a poloidal projection of the neutron emissivity. This projection is assumed to be toroidally symmetric but, unlike most TRANSP outputs, is not flux-surface averaged, a point that is important when interpreting the results from the NC [25]. The LINE2 code [20] uses this neutron emissivity projection to model the full profile of the expected neutron emission rate measured by the NC in any particular position. The amplitude of the computed profile is the only free parameter in the calculation and can be thought of as the NC's detection efficiency. In practice, the detector efficiency for all four channels has been independently determined to be 0.08 ± 0.02 [8] and the 'free' parameter in the LINE2 calculation is expected to be close to this figure (in the absence of MHD influences on the FI population). NC profiles have been calculated in this way for the eight shots of the power/density scan using the outputs from the TRANSP simulations. In the experiments performed, only the highest density single beam discharge (29195) was determined to be completely free of MHD and redistribution effects during the POI (as demonstrated in figure 4(*a*)). Therefore, this shot was used to determine the efficiency factor of the two midplane NC channels such that measurements from all eight shots may be compared with the calculations in a consistent manner. The detector efficiency factors calculated in this way were found to be 0.08 for both midplane viewing chords.

Figures 4(*b*) and (*c*) shows the results of this exercise. Once again, the comparison between the measured and calculated neutron count rate is averaged over the POI and expressed as the ratio (measured neutron rate)/(calculated neutron rate). The error bars indicate the combination of the uncertainty in the NC count rate inherent to the detectors and the standard deviation of the average over the POI. These sources of error are additive as the first is due to the characteristics of the instrument and the second is due to temporal variations in the plasma. In all eight shots, the NC was in the same position such that its midplane chords had impact parameters (i.e. tangency radii) of 0.95 m and 1.14 ± 0.03 m. These will be referred to in the following discussion as on-axis and off-axis, respectively. It is finally noted that the off-axis measurement for shot 29034 (mid–low density, one beam) was determined to be faulty so has been omitted from this particular analysis.

In agreement with the FC results, the ratio for the on-axis chord (figure 4(*b*)) decreases with decreasing plasma density and the values of the ratio are similar to the FC results at each plasma density level. The error ranges are of a magnitude such that it cannot be said with any certainty that there is

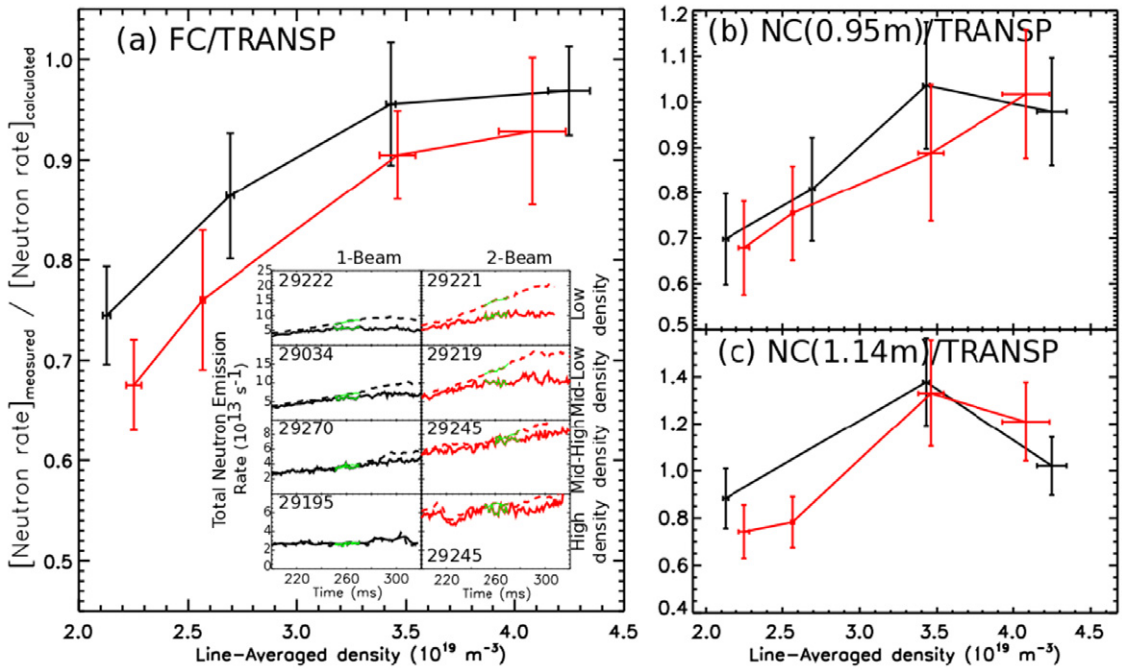

Figure 4. (*a*) (Inset) Neutron emission rate measured by the FC (solid) and calculated by TRANSP (dashed) with indicated POI (green) for each time trace. (*a*) (Main panel) FC measurement divided by TRANSP calculated neutron emission rate averaged over the POI plotted versus line-averaged density; black = one-beam shots, red = two-beam shots. (*b*) NC measured neutron count rate divided by TRANSP calculated neutron rate averaged over the POI for NC line of sight with $R_T = 0.95$ m. (*c*) NC measured neutron count rate divided by TRANSP calculated neutron rate averaged over the POI for NC line of sight with $R_T = 1.14$ m.

an apparent trend for decreasing ratio with increasing power though such a trend is not precluded by this analysis. The neutron emission ratio for the off-axis chord (figure 4(*c*)) also exhibits a decrease in the ratio at low plasma density though at the mid–high plasma density level ($\sim 3.4 \times 10^{19}$ m^{-3}) the ratio for the off-axis viewing chord is above unity for both power levels. A possible explanation is that, at this density level, the FI redistribution effect is acting in such a way as to increase the density of fast particles at the radius observed by this chord. Unfortunately, further investigation of this observation is not possible with the data set available.

Examination of the edge D_α signal for the eight shots in the power/density scan has shown that some, but not all, FB modes are correlated with positive spikes in the D_α emission, which is interpreted as a loss of particles from the plasma [26]. Spikes in D_α emission correlated with FB modes are observed for all of the two-beam shots indicating FI losses. For the one-beam shots, only some of the FB modes are correlated with spikes in D_α emission and only for the two lower densities. Since all FB modes are accompanied by drops in the neutron emission signal, it can be stated that FI losses result from FB modes in the two-beam shots but that FB modes in the one-beam shots sometimes result in FI losses and redistribution but only redistribution at higher density.

TRANSP has the facility to output the full FI distribution function at specified times during the simulation. The FI distribution function has thus been obtained for each shot in the power/density scan at 250, 260 and 270 ms (260, 270 and 280 ms for shot 29251). The intention was then to use these FI distribution functions to obtain estimates of the gradient of the distribution with respect to $-e\Psi_p$ i.e. the simplified form of the toroidal canonical angular momentum defined in section 3.1. Neglecting the stabilization of the FB modes due to the energy gradient in the FI distribution function, the magnitude of the radial gradient can be assumed to be approximately representative of the magnitude of the drive for the observed FB modes or, in the cases where no FI redistribution was observed, to represent a critical magnitude below which FI redistribution by FB modes is suppressed. Making the assumption that the shots in the scan have sufficiently similar q-profiles, the magnitude of the $\partial f/\partial \psi_p$ term calculated for each shot may be directly compared to assess the relative magnitude of the FB drive throughout the scan. Examination of the q-profiles derived from EFIT++ using magnetic, kinetic and MSE constraints shows this to be a reasonable assumption.

The point in the FI distribution function at which the radial gradient should ideally be assessed is at the radial location of the mode and at the pitch angle and energy of the particular resonance primarily driving the mode. Determination of the mode location in this parameter space could be done, for example, with reference to an MHD stability code such as MISHKA [27]. Precise determination of the modes' location using this methodology presents some difficulty due to the inherent uncertainty in obtaining the q-profile. The MSE constraint used in the EFIT++ equilibrium, being an experimentally measured quantity, has measurement errors associated with it. To determine the effect of these errors on the resultant q-profile, a number of EFIT++ equilibria were calculated whilst varying the MSE data within its error bounds. The resultant ensemble of q-profiles obtained thus represents the extent of the uncertainty in q due to the measurement errors in the MSE data, which was determined to be ± 0.1. Since the q-profile in these plasmas tends to be rather broad

and with low magnetic shear over a large radial extent, the uncertainty means that the $q = 1$ surface could be located anywhere in the region $0.0 < \Psi_{p,N} < 0.4$ (where $\Psi_{p,N}$ is normalized poloidal flux). Previous studies which included examination of the FB mode stability [26, 28] have additionally shown the FB mode eigenfunctions in MAST are very broad, encompassing a similar radial range as that determined for the $q = 1$ surface location. Assessment of the FB mode stability by theory-based modelling is very sensitive to the q-profile so attempts at stability assessment in these cases could not be expected to locate the radial position of the FB mode any more accurately than the range determined for the location of the $q = 1$ surface.

Given these limitations, an alternative approach was adopted in order to calculate a relevant value of the radial gradient of the FI distribution for each shot such that a comparison may be made. First, a small level of smoothing was applied to the FI distribution function to reduce noise in the calculated gradient due to the finite number of MC particles used in the simulations. The smoothing used a simple boxcar operator with a window width of 2.5 keV in energy space, 0.08 in pitch-angle cosine space and 0.1 in normalized $\Psi_{pol,N}$ space. The magnitude of $\partial f/\partial\psi_{p,N}$ was then assessed over all pitch-angle space, within the radial region $0.0 < \Psi_{p,N} < 0.4$ along the outboard midplane and within the energy range $50\,\text{keV} < E < 60\,\text{keV}$. Given the similarity of the plasmas in the power/density scan, it is reasonable to assume that particles of similar energy in each case are responsible for driving the observed FB modes in all eight shots. Therefore the analysis was constrained to the specified energy range in which the peak of the FI distribution is found at the radii under investigation.

The maximum value of the radial gradient found within this region was then taken as representative of the magnitude of the drive for the FB modes. To account for the fact that the FB mode may be located anywhere within the specified radial region, the standard deviation of the quantity $\partial f/\partial\psi_{p,N}$ in the region $0.0 < \Psi_{p,N} < 0.4$ was taken to represent the uncertainty in the magnitude of the radial gradient. Since the uncertainty is estimated over the full range of possible locations for the FB mode, comparisons of the magnitude of $\partial f/\partial\psi_{p,N}$ in different shots may be made with a reasonable degree of confidence having accounted for the uncertainty in mode location.

The two shots in the scan with one beam and at the higher plasma density levels were shown to be consistent with operation without FI redistribution. The larger of the values of $\partial f/\partial\psi_{p,N}$ found in these two shots can therefore be assumed to represent a critical level below which FB modes of sufficient amplitude to cause FI redistribution are suppressed. To account for the uncertainty in the mode location, the critical value of $\partial f/\partial\psi_{p,N}$ is set to the lowest extent of the uncertainty range of the mid–high density shot (29270). This essentially recognizes that the magnitude of the gradient driving the FB mode may be as small as the lowest extent of the uncertainty range calculated for this shot. In section 4 of this work, modifications to the NBI system for MAST-U are discussed with the intention of reducing the magnitude of the FB drive. Taking the maximum values for $\partial f/\partial\psi_{p,N}$ in the MAST-Upgrade scenarios therefore represents a pessimistic approach in that the drive for the FB modes in these plasma scenarios may actually be smaller than that calculated. Then comparing these maximum values with the lower end of the uncertainty range from shot 29270 represents a robust comparison since the drive for the FB mode in this plasma may be larger than this minimum. Use of maximum values for assessment of $\partial f/\partial\psi_{p,N}$ is therefore justified in that any value of $\partial f/\partial\psi_{p,N}$ calculated later in section 4 for MAST-U which is below the specified critical level is indicative the FI redistribution is likely to be avoided having accounted as far as possible for uncertainties in the experimental analysis.

The results of this analysis are shown in figure 5(*a*). It is first noted that the radial location of the maximum of the radial gradient for all the shots in this investigation was found to be within the region $0.94\,\text{m} < R < 1.01\,\text{m}$, i.e. just outboard of the magnetic axis, and in the pitch-angle cosine range $0.5 < \frac{v_{||}}{v} < 0.8$. This is deemed reasonable since, in the next section, evidence is presented that shows the radial location of the greatest effect of the FB modes on the neutron emission is at a similar radial location. The principal result from inspection of figure 5(*a*) is the larger magnitude of $\partial f/\partial\psi_{p,N}$ at lower plasma densities compared with the points at higher plasma densities. Since the uncertainty bounds of the high and low plasma density points do not overlap, it is concluded that $\partial f/\partial\psi_{p,N}$ is indeed larger in the low plasma density cases. It is further noted that the high NBI power shots exhibit larger magnitude radial gradients than the corresponding low NBI power shot at similar plasma density. This conclusion is robust for the two high plasma density levels as the uncertainty ranges do not overlap, but is uncertain at the two lower plasma density levels due to the uncertainty ranges for these points.

In previous studies [28] estimates of the position of the FB resonances in $(R, Z, E, \frac{v_{||}}{v})$ parameter space were made for similar plasmas using the wave–particle interaction code HAGIS [29]. This exercise was repeated for a representative plasma equilibrium based on pulse 29222 (i.e. the one-beam low plasma density shot) at $t = 0.26\,\text{s}$. The intention of this assessment was to check that FB resonances exist in a similar part of the distribution function to the region in which the maxima of the quantity $\partial f/\partial\psi_{p,N}$ has been located in the analysis described above. The HAGIS calculations indicate the FB resonance condition is satisfied by co-passing FIs at all energies from the thermal up to the NBI injection energy close to the trapped/co-passing particle boundary in energy/pitch-angle space. The precise location of this boundary varies with radius in the range $0.1 < \frac{v_{||}}{v} < 0.6$ in the radius range under consideration ($0.0 < \Psi_{p,N} < 0.4$) so is in approximate agreement with the region of the FI distribution function in which the maxima of $\partial f/\partial\psi_{p,N}$ have been found. It is recognized, however, that such resonance calculations are strongly affected by the q-profile and particularly the position of the $q = 1$ surface. Since the position of $q = 1$ is subject to uncertainty as stated above, no further use was made of the HAGIS resonance maps other than to check FB resonances exist in these plasma equilibria and that the results presented exist in similar parts of the parameter space. A particular point to note from this exercise is that FB resonances exist over the whole energy range. The analysis was therefore repeated a number of times constraining the energy range to different values ($0\,\text{keV} < E < 10\,\text{keV}$, $10\,\text{keV} < E < 20\,\text{keV}$, ..., $40\,\text{keV} < E < 50\,\text{keV}$). It was found that the result in each case was similar to that shown in figure 5(*a*)

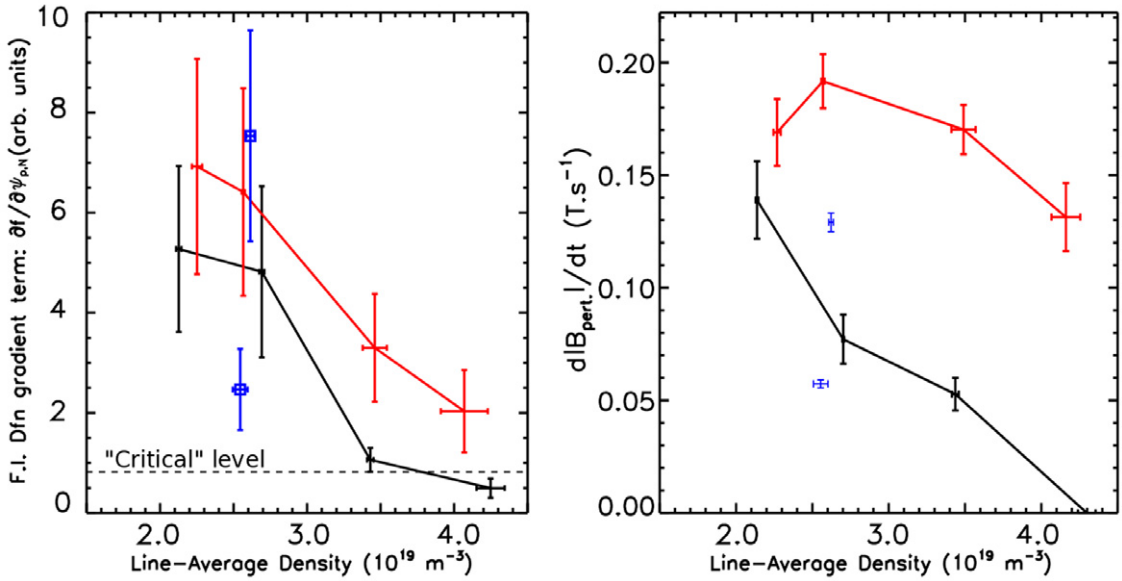

Figure 5. (*a*) FI distribution function gradient $\partial f/\partial\psi_{\mathrm{p,N}}$ (plotted with arbitrary units) averaged over POI; black: one-beam shots, red: two-beam shots. Also shown for comparison are the one- and two-beam shots carried out in previous experiments reported in [6]. The indicated 'Critical' level is the level above which FB modes should be expected to cause FI redistribution. (*b*) Mode growth rate $\mathrm{d}\left|B_{\mathrm{pert.}}\right|/\mathrm{d}t$ versus line-averaged density for black : one-beam shots, red : two-beam shots, blue : one- and two-beam shots carried out in previous experiments reported in [6].

i.e. that larger values of the radial gradient are found for shots with higher NBI power and/or at lower plasma density. For the energy intervals below 20 keV, the uncertainty ranges became larger such that the results at these energies are inconclusive. This is due to the lower number of particles in the lower energy region of the distribution function and thus a higher MC noise level in the calculated radial gradient. It is therefore considered that the conclusion drawn from inspection of figure 5(*a*) is not dependent on the energy range chosen for the analysis.

In the earlier study by Turnyanskiy *et al* [6], a one-beam/two-beam pair of shots at the same plasma density was obtained. The original analysis of these shots used an *ad hoc* anomalous FI diffusion term (D_{an}) in the TRANSP modelling to characterize the magnitude of the FI redistribution (and which is discussed further in [24]). This indicated a low level of FI redistribution for the one-beam shot (shot number 26887: $D_{\mathrm{an}} = 0 - 1\,\mathrm{m}^2\,\mathrm{s}^{-1}$) and much higher level for the two-beam shot (shot number 26864: $D_{\mathrm{an}} = 2 - 3\,\mathrm{m}^2\,\mathrm{s}^{-1}$). This pair of shots has been re-analysed to obtain the FI distribution functions from NUBEAM using the method described above such that comparison can be made with the eight shots of the present study. The results for these two shots are shown as blue squares in figure 5(*a*) and are consistent with the present study, i.e. the maximum values of $\partial f/\partial\psi_{\mathrm{p,N}}$ obtained are comparable to the present study. Also, the magnitude of $\partial f/\partial\psi_{\mathrm{p,N}}$ for the two-beam shot is significantly larger than for the one-beam shot, also in agreement with the present study.

The relative magnitudes of the FB drive term can now be compared with the observed growth rate of the FB mode in each case. As part of the standard data, the MAST magnetics team provide an estimate for the absolute value of the magnetic perturbation ($B_{\mathrm{pert.}}$) due to MHD modes in the plasma. The time derivative of this signal was therefore used to estimate the maximum value of the growth rates for all FB modes that occurred during the POI in each shot. In those shots in which more than one FB mode occurred during the POI, an average growth rate has been calculated. The results are plotted in figure 5(*b*) versus the line-averaged density and are grouped into one-beam and two-beam shots. No modes occurred during the POI for the highest density one-beam shot (29195) so this data point has been set to zero. The error bars for the growth rate represent the standard deviation of the calculated growth rate in a 50 μs wide window centred on the point at which the growth rate of the mode reaches its maximum value. The error bars for the density data represent the standard deviation of the line-averaged plasma electron density during the POI. The trends in the FB mode growth rate are seen to be consistent with the $\partial f/\partial\psi_{\mathrm{p,N}}$ estimates, i.e. that higher power and/or lower density shots which exhibit higher values of $\partial f/\partial\psi_{\mathrm{p,N}}$ also exhibit larger mode growth rates. It is noted that the mode growth rate for the lowest density two-beam shot shows a slightly lower value than expected. The estimated error bounds on $\partial f/\partial\psi_{\mathrm{p,N}}$, however, mean that this point is not inconsistent with the gradients in the calculated FI distribution. Data points from the previous experiments by Turnyanskiy *et al* [6] are again included on this plot and are seen to be generally consistent with the present study; the growth rate in the two-beam shot is significantly larger than in the one-beam shot and both are of comparable magnitude to the results from the present study. Such correlation between mode amplitude and the magnitude of the redistribution/loss of FIs is consistent with previous studies [30].

These modelling results taken together provide a coherent explanation of the relationship between the magnitude of the FI redistribution observed and the position of the data point in the power/density parameter space. Essentially, lower plasma density and/or higher NBI power leads to a larger value of the MHD drive term in equation (1). This is followed by a

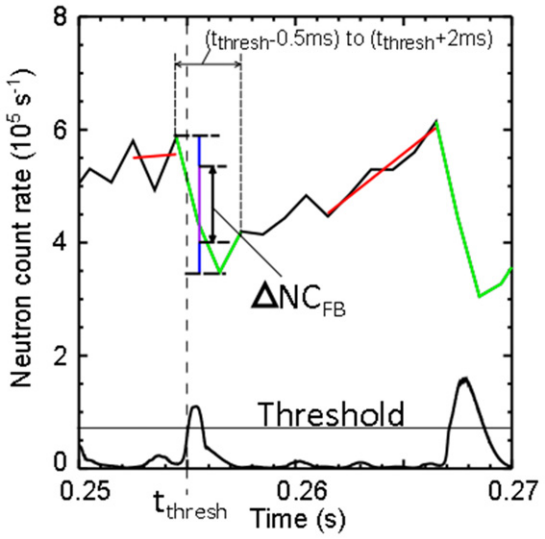

Figure 6. An illustration of the analysis method to determine the quantity ΔNC_{FB}. See the text for details.

generally higher observed value of the mode growth rate which is then followed by a larger magnitude redistribution effect as determined by the deficit in the measured neutron production rate compared with the modelled neutron production rate.

3.3. Empirical evidence for core localization of FI redistribution effect

3.3.1. Neutron camera. The FB modes observed during the POI are thought to be localized to the plasma core and ascertaining the radial extent of their influence on the FI population is one of the subjects of this investigation. Since both the NC and FIDA systems have good spatial resolution it has been possible to determine the spatial extent of the FI redistribution effect of the FB modes using these diagnostic data.

As described earlier, NC position scans were performed in a series of repeated shots at the highest and lowest plasma density levels. In the low plasma density case, five shots were performed, which were nominally identical apart from the viewing position of the NC, giving a total of ten spatially separated chords on the midplane. In the high plasma density case, six shots were performed giving 12 chords. In the high plasma density scan, small FB modes were observed during the POI in three of the six shots. However, the effect on the neutron emission rate at the time of these modes was comparable to the noise level in the measurement hence no statistically significant result could be determined and the high plasma density case was deemed free of FI redistribution effects, in confirming the result in section 3.2 at this NBI power and plasma density. In the low plasma density case, however, the neutron emission rate was somewhat higher and the FB modes were of larger amplitude producing drops in the NC count rate much larger than the noise. The FB modes occurred during similar time intervals in all five shots of the low plasma density scan so detailed analysis of the NC data from the various lines of sight over the POI has been carried out to determine the spatial effect of the FB mode on the FI population.

For each viewing chord position in the scan, the analysis method illustrated in figure 6 was followed. Firstly, the onset time of each FB mode during the POI was determined by setting a threshold in the amplitude of the rms of the LFS-MC signal; the time at which the signal reached this amplitude was labelled t_{thresh}. Examination of the LFS-MC signal determined that the FB modes typically started approximately 0.5 ms before the modes reached this amplitude and were typically of 2.5 ms duration. This period, $(t_{\text{thresh}} - 0.5\,\text{ms}) < t < (t_{\text{thresh}} + 2.0\,\text{ms})$ was taken to be representative of the period during which the FB mode was affecting the FI population. These '*intra*-FB' periods are highlighted in green in figure 6. The start and end times of '*inter*-FB' periods (i.e. the periods between FB_i and FB_{i+1} in which no redistribution effect was occurring) were defined by $\left(t_{\text{thresh},i} + 5\,\text{ms}\right) < t < \left(t_{\text{thresh},i+1} - 0.5\,\text{ms}\right)$, i.e. 5 ms after the start of one FB to the start of the next. The start and end time of the POI make the final boundaries of the inter-FB assessment periods (unless the start/end times happen to be defined as being within intra-FB periods). These periods are illustrated by red lines in figure 6 and the average over these periods, taken to represent the unperturbed neutron emission rate, is referred to below as NC_{AV}.

The drop in neutron rate due to the effect of a particular FB mode was then determined by examination of the signal during the intra-FB periods as

$$\Delta NC_{FB} = \max\left(NC_{\text{intra-FB}}\right) - \min\left(NC_{\text{intra-FB}}\right) - \left(\sqrt{2NC_{\text{std}}^2}\right) \quad (2)$$

where the final term is the combination in quadrature of the statistical uncertainty in the neutron count rate at the maximum level (i.e. the maximum of the NC count rate during the intra-FB period) and at the minimum level (i.e. the minimum of the NC count rate during the intra-FB period). Inclusion of this final term accounts for the uncertainty in the magnitude of the neutron emission signal ensuring that the final value for ΔNC_{FB} is a reasonable evaluation of the drop in the signal due to the FB and not simply an artefact of the noise in the signal. The statistical uncertainty was assessed using the inter-FB periods in the time interval 250–270 ms in shot 29222 and was found to be 10.5% of the signal level. The value of the statistical uncertainty was therefore set to $NC_{\text{std}} = 0.105 \times \max\left(NC_{\text{intra-FB}}\right)$. The value of ΔNC_{FB} is indicated in figure 6 for the first of the FB modes in this POI in which the subtraction of the final term in the above expression is indicated by the vertical blue lines above and below the resultant ΔNC_{FB}. For shots in which more than one FB event occurred in the POI, the average value of ΔNC_{FB} for all events was taken as a representative single value for that NC chord. For those FB events in which the error exceeded the difference between the maximum and minimum emission rate, i.e. in which $\Delta NC_{FB} \leqslant 0$, the value was set to zero.

The proportional drop in neutron emission was then finally computed as $\Delta NC_{FB}/NC_{AV}$ for each of the NC chords. The error in the final value was taken to be $\sqrt{2NC_{\text{std}}^2 + NC_{\text{AV,std}}}$ where the first term represents the error in determining the magnitude of the drop in the neutron rate and the final term the error in determining the average of the inter-FB signal. Ideally, the FB modes would be spaced sufficiently that the neutron

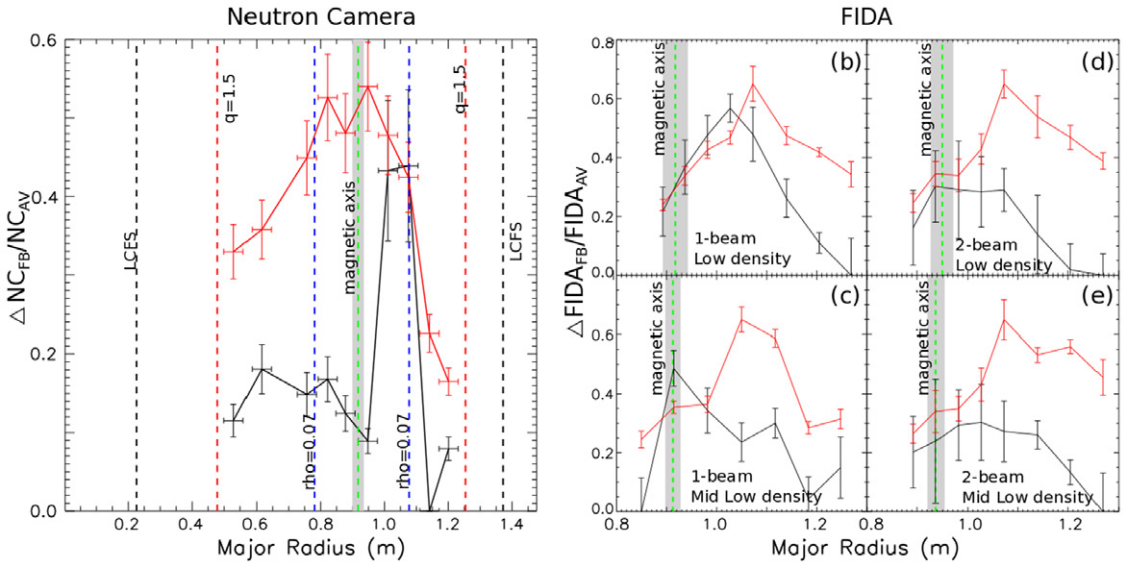

Figure 7. (*a*) Relative drop in neutron rate due to FBs as a function of NC viewing chord tangency radius (solid black line and data points), normalized neutron emission rate (solid red line and data points, arbitrary scale). Representative quantities from MSE-constrained EFIT are shown as follows (in the case of flux surface quantities the midplane major radius is shown): magnetic axis (vertical green dashed line), $\psi_{\mathrm{p,normalized}} = 0.07$ (vertical blue dotted line), $q = 1.5$ (vertical red dashed–dotted line), LCFS (vertical black dashed line). MAST pulses used in obtaining profile: 29222, 29924, 29928, 29929, 29931. (*b*)–(*e*) Relative drop in FIDA emission due to FB modes for the one-beam and two-beam shots at the two lower density levels in the scan (black line and data points). FIDA emission (red line and data points, arbitrary scale). Also shown is the position of the magnetic axis from MSE-constrained EFIT.

emission rate could return to its completely unperturbed level before the next FB mode again affects the FI population. In the example shown, it is apparent that this is not the case so the estimate of signal noise, $\mathrm{NC_{AV,std}}$, is probably an overestimate since it necessarily includes some of the recovery period of the FI population. This overestimate of the error actually serves to strengthen the following conclusions since, even with the larger errors, the drops in the neutron emission rate are still large enough to provide evidence of the localization of the effect on the FI population. It is noted that, in the shots analysed, every FB mode resulted in drops in the neutron rate for every line of sight of the NC. This indicates a loss of FIs from this region of the plasma though spikes in edge D_α emission are only observed for some of the FB modes in this scan. This indicates a combination of FI redistribution accompanied by, in some cases, FI losses.

The result of this analysis is shown in figure 7(*a*) where the black data points are $\Delta\mathrm{NC_{FB}}/\mathrm{NC_{AV}}$ as a function of the impact parameter (i.e. tangency radius) of the NC viewing chords. Also shown is the profile of the measured neutron emission rate (red data points, plotted on an arbitrary scale) to illustrate that the proportional drop in neutron emission cannot simply be reproduced by scaling the neutron emission rate. Various plasma equilibrium quantities have been taken from an MSE-constrained EFIT equilibrium and are displayed on the graph along with the NC data. Assessment of uncertainties in the EFIT equilibrium has not been carried out so no ranges of values are shown for these positions though it is recognized that there will be some uncertainty in their radial locations. The midplane radius values of the plasma boundary are indicated by vertical dashed black lines and the radial position of the magnetic axis is shown by a vertical dashed green line (the standard deviation of the variation in the position of the magnetic axis throughout the POI is indicated by the grey region though this is only due to temporal variation in the equilibrium calculation and does not contain any uncertainty estimates for the equilibrium calculation itself). The radial position of the $q = 1.5$ surface is also shown. It is clear therefore that all NC chords examined have tangency radii well within the $q = 1.5$ surface. No $q = 1$ surface was determined by MSE-constrained EFIT for these shots, however $n = 1$ FBs are associated with a $q = 1$ surface. It is therefore probable that the q-profile drops to a value less than or equal to 1 in these plasmas during the POI and this is consistent with the typical error in the EFIT derived q-profile stated earlier.

Of particular note in this graph is the large localized peak at $1.0\,\mathrm{m} < R < 1.1\,\mathrm{m}$ indicating that the FB mode is having a proportionally larger effect on the FI population in this region as compared with the rest of the profile. This is therefore interpreted as evidence that the effect of the FB mode is localized in the plasma to a defined region just outside the magnetic axis. The observation that the magnitude of $\Delta\mathrm{NC_{FB}}/\mathrm{NC_{AV}}$ has a local minimum at the magnetic axis where the neutron emission rate itself has a local maximum, as well as the fact that $\Delta\mathrm{NC_{FB}}/\mathrm{NC_{AV}}$ decreases with radius more rapidly than the neutron emission rate, also leads to the conclusion that the peak in $\Delta\mathrm{NC_{FB}}/\mathrm{NC_{AV}}$ is not simply a consequence of a lower level of neutron emission at larger radii but is genuinely due to the effect of the FB mode on the FI population being stronger at particular radius.

Interestingly, there is a second local maximum in the $\Delta\mathrm{NC_{FB}}/\mathrm{NC_{AV}}$ data on the high-field side (HFS) of the magnetic axis at $R \sim 0.75\,\mathrm{m}$. Examination of the full magnetic flux reconstruction from EFIT indicates that the maxima are located at similar values of normalized poloidal flux (the position of $\psi_{\mathrm{p,N}} = 0.07$ is shown by a blue vertical dashed

line). It is also noted that the peaks are highly asymmetrical with the peak on the LFS being much larger than on the HFS. A possible explanation concerns the geometry of the lines of sight of the NC. If a line of sight has a tangency radius on the LFS of the magnetic axis then it only sees the LFS of the plasma. If the tangency point is inboard of the magnetic axis, it looks through the LFS as well as at the HFS. Measurements from such lines of sight will therefore show a combination of neutron emission from the LFS as well as the HFS. However, since the line of sight has a shorter path length in the LFS of the plasma compared to a chord with larger tangency radius, any line-integrated measurement due to LFS activity will be of lower amplitude. Since the HFS peak in figure 7(*a*) is of lower amplitude, it is certainly possible that this is the explanation for the presence of this peak, i.e. a relatively steady but lower amplitude neutron emission rate from the HFS compounded with the large drops in neutron emission rate from activity on the LFS. The present analysis offers no explanation for the asymmetry of the effect of the FB mode on the HFS and LFS. It is possible that there is a larger effect of the FB modes on the trapped particle population compared to the passing particles. Since there is a relatively large trapped particle population on MAST (up to 60% at $\psi_{p,N} = 0.07$ from the TRANSP calculations), which is asymmetrical between the HFS and LFS, this may account for the observations though explanation of the asymmetry will require further study and is the subject of ongoing enquiry.

The detailed analysis presented here of the low-density one-beam case can be compared with the two-point analysis shown in figures 4(*b*) and (*c*) for the other NBI power and plasma density levels in the scan. First it is noted that the points in figures 4(*b*) and (*c*) representing the one-beam low plasma density shot are consistent with the analysis shown in figure 7(*a*). Even though the 0.95 m line of sight corresponds to a local minimum in figure 7(*a*), this is still consistent with the error range of the ratio for this point in figure 4(*b*). It is noted that a line of sight with major radius 1.05 m corresponding to the position of the local maximum in figure 7(*a*), would produce a data point in figure 4(*b*) with ratio ~0.58 indicating a larger effect on the FI population at this radius than at 0.95 m. Data for radius 1.05 m are only available for the low NBI power/low plasma density point in the scan so it is not possible to produce equivalent graphs to figures 4(*b*) and (*c*) for any other radii.

It is also noted that the radius at which the FB modes have largest effect on the neutron emission rate is slightly larger than the radius at which the maximum in the radial gradient of the FI distribution function was found in section 3.2. This implies that the magnitude of the $\partial f/\partial \psi_{p,N}$ term may be an overestimate (since the FI distribution peaks in the centre of the plasma) but that, as stated earlier, any subsequent mitigation found from modified beam geometry, which is the point of the work described in section 4, will be robust against the uncertainty in the estimation of $\partial f/\partial \psi_{p,N}$.

3.3.2. Fast-ion D_α. The FIDA diagnostic recorded data for the eight shots of the power/density scan using core orientated toroidal lines of sight. The FIDA data have been processed to obtain the proportional drop in the FIDA signal due to the FB modes in the same way as the NC data described above. The FIDA signal suffered from relatively higher noise than the NC and the signal intensity decreased markedly with increasing plasma density, as is expected from the physics of FIDA spectroscopy. The FIDA data at the two highest plasma density levels were therefore unusable, exhibiting an unacceptably low signal to noise ratio but the data from the four shots at the two lower plasma density levels contain useful information. The analysis of the one- and two-beam shots at the two lower plasma density levels is shown in figures 7(*b*)–(*e*). In these graphs, the black data points indicate the proportional drop in the FIDA signal due to FBs during the POI, plotted versus the tangency radius of the FIDA lines of sight. The red data points show the absolute value of the FIDA signal (plotted on an arbitrary vertical scale) as a function of the tangency radius. The error bars represent the standard deviation in the signal over the POI. The vertical green line indicates the position of the magnetic axis as determined by MSE-constrained EFIT (the grey region indicates the standard deviation of this position over the POI).

Comparison of the absolute FIDA signal and the proportional drop once again indicates that the drop in the signal due to FBs cannot simply be reproduced by scaling the FIDA emission signal so contains information about the relative effect of the FB on the FIDA emission. Even in the case of the lowest plasma density one-beam shot (figure 7(*b*)) where this could be a valid interpretation at $R < 1.1$ m, the lines diverge rapidly for values of $R > 1.1$ m. Although the errors in the proportional-drop analysis are generally larger for FIDA than for the NC, the conclusion can still be drawn that FI redistribution due to FBs has a greater effect close to the magnetic axis, i.e. in the core of the plasma, than at larger radii ($R > 1.1$ m) even though a substantial FI population exists at larger radii as indicated by the magnitude of the FIDA emission at $R > 1.1$ m. This analysis is therefore in qualitative agreement with the NC analysis in the previous section and provides further evidence for the core localization of the effect of FB modes on the FI population using a diagnostic technique that is completely independent of the neutron emission analysis discussed previously. Since both the FIDA and the neutron diagnostics are sensitive to the higher energy range of the FIs (>44 keV), it is expected that the results from these two diagnostics should give similar results as is seen from comparison of figure 7(*a*) with figures 7(*b*)–(*e*).

4. Implications for MAST-Upgrade scenarios

A significant upgrade to MAST is currently under construction [2, 3] that will bring increased capabilities to the experiment, such as off-axis NBI heating and current drive, increased toroidal field and increased pulse duration as well as testing the novel Super-X divertor concept. The off-axis NBI current drive (NBCD) is intended to allow a certain degree of control of the q-profile with the intention of creating plasma scenarios with current profiles tailored to avoid deleterious MHD modes. In the Core-Scope (CS) upgrade, due to be operational in 2015, the NBI system will consist of two injectors, one located with the same injection geometry as those currently installed on MAST (referred to hereafter as the 'on-axis' position), the other located with a horizontal line of sight 650 mm above the midplane (referred to hereafter as the 'off-axis' position).

This combination will provide efficient core heating, via the on-axis injector, and significant off-axis heating and NBCD via the off-axis injector.

The specifications of these injectors are energy up to 75 keV and power up to 2.5 MW. In the experiments described earlier, the two-beam shots had on-axis injected power of around 3 MW, a similar level to the maximum achievable on-axis power in the MAST-Upgrade CS. Following from the experimental results presented in section 3, the implication of operation of the on-axis MAST-Upgrade beam at full power is that FI redistribution via FB modes is likely to occur at low plasma density. Since one of the purposes of the NBI configuration on MAST-Upgrade is to allow q-profile tailoring, uncontrolled redistribution of the FI population by MHD would then limit the degree of control that can be effected by the re-positioned NB injector. Development of steady-state plasmas, in which the plasma current is maintained by fully non-inductive current drive for a period of several current diffusion times, will be important for future spherical tokamak applications. A significant proportion of this non-inductive current is intended to be provided by NBCD which will require operation at low density. As the results in this study have shown, operation at low density is incompatible with avoidance of FB modes and redistribution of the FI population. However, these results also suggest a strategy for modification of the NBI system that will be installed in later stages of the upgrade that should produce significant mitigation of the FB modes responsible for the observed FI redistribution.

In the staged construction plan for MAST-Upgrade, the principal modification in moving beyond CS will be the addition of a new beamline called the double beam box (DBB) which will give the capacity for an extra on-axis beam at the midplane and/or an extra off-axis beam 650 mm above the midplane. Throughout the design of MAST-Upgrade, physics assessments of the expected performance of the plasma using different assumptions of engineering geometry and capability have been carried out using TRANSP. These simulations were set up using carefully selected temperature and density profiles that are expected to be achieved in MAST-Upgrade together with realistic plasma shapes that can be produced with the MAST-Upgrade poloidal field coil set [2, 3, 31]. Two representative plasma scenarios are used with Greenwald density levels $n_0/n_{GW} = 0.58$ and $n_0/n_{GW} = 0.23$, identified as scenarios A1 and A2 respectively, where $n_{GW} = I_p/\pi a^2 \left(10^{20}\,\mathrm{m}^{-3}\right)$, I_p is the plasma current in MA, a is the plasma minor radius in metres and n_0 is the electron density at the magnetic axis. The high plasma density scenario, A1, is used to assess performance in a standard H-mode whilst the low-density scenario, A2, is used to assess maximum expected current-drive capabilities of the NB system and potential NB shine-through issues. In all simulations, the electron temperature was adjusted in order to achieve an H-factor of 1 ± 0.03 according to the IPB98(y,2) H-mode scaling [32].

The MAST-Upgrade simulations differ from the experiments discussed in section 3 in that they are carried out with a plasma current of 1 MA and $B_0 = 0.785$ T compared to 0.8 MA and $B_0 = 0.585$ T. However, the plasma current does not significantly affect the FB stability calculation [21] and the ratio I_p/B_0 in the two cases is similar, differing by only 7%. Examination of the q-profiles from the MAST-Upgrade TRANSP simulations indicate that at low n_0 in MAST-Upgrade ($n_0 < 5 \times 10^{19}\,\mathrm{m}^{-3}$), a $q = 1$ surface exists in the plasma so FB mode resonances can be expected. Furthermore, the approach to assessing the magnitude of the FB mode drive term from equation (1), as explained in section 3, encompasses a large radial region of the plasma and the uncertainty estimate accounts for uncertainty in location of the FB mode. The location of the $q = 1$ surface in the low-density MAST-Upgrade plasmas is at a smaller radius than the maximum extent of the radial range over which the uncertainty in the radial gradient is assessed (according to the TRANSP prediction). The analysis method is therefore considered sufficient to account for uncertainty in the radial location of FB modes that may occur in these plasma scenarios. Given also that the maximum of the magnitude of the FB mode drive term is compared with the minimum of the range calculated for shot 29270 (one-beam, mid–high plasma density), the comparisons that will be shown in this section between the MAST and MAST-Upgrade TRANSP simulations are considered valid for the purpose of assessing whether FB modes are likely to occur in MAST-Upgrade plasmas and the effect of modifying the NBI geometry.

FI distribution functions from the representative TRANSP runs available for MAST-Upgrade have been assessed using the same methodology described in section 3.2 but using the energy range 50 keV $< E <$ 75 keV to account for the higher NB injection energy used in the MAST-Upgrade simulations. The results of this study are shown in figure 8 (main panel). This diagram is essentially the same as that shown earlier in figure 5(a) with additional data points representing the results from the assessment of various MAST-Upgrade plasma scenarios and NBI injector combinations and geometries. The green triangles show the representative magnitudes for $\partial f/\partial \psi_{p,N}$ of the CS scenarios A1 and A2. The point at high plasma density (scenario A1) clearly lies in the region in which the FI population should be unaffected by FI redistribution but at low plasma density (scenario A2), FB modes and subsequent FI redistribution is likely. The red triangles indicate the expected magnitudes for $\partial f/\partial \psi_{p,N}$ in a future upgrade design (i.e. the CS arrangement with an extra off-axis injector). In this case the magnitude of $\partial f/\partial \psi_{p,N}$ has increased in both the low and high density scenarios. The point representing the low-density scenario now suggests FB modes with a stronger FI redistribution effect are likely and even for the high-density scenario, the error range crosses the 'critical' level such that FB modes causing FI redistribution may occur. The red triangle at low density is actually an underestimate since, in order to allow the TRANSP simulation to run successfully, it was necessary to reduce the power of the on-axis injector to 1.5 MW in this simulation (see 2.5 MW in the other MAST-Upgrade simulations). This point should therefore have a higher value of $\partial f/\partial \psi_{p,N}$ (if the on-axis beam were to be run at full power) and correspondingly larger amplitude FBs and FI redistribution.

In reality, it may well be the case that higher on-axis power will cause higher density peaking than has been assumed. The electron density profiles used in the MAST-Upgrade simulations are extremely flat and the difference between the low and high density cases is a simple scaling factor, i.e. no change to the density peaking factor has been included. This is a fair assumption since MAST-Upgrade will operate in H-mode

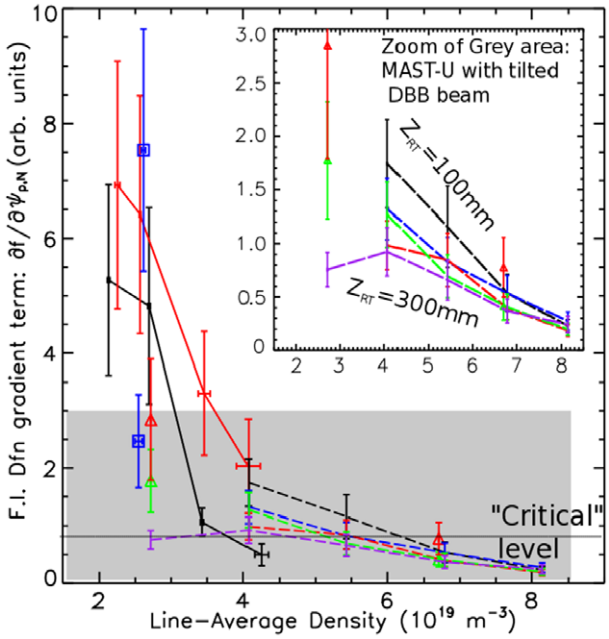

Figure 8. Maximum gradient $\partial f/\partial\psi_{\mathrm{p,N}}$ (plotted with arbitrary units, as in figure 5(*a*)) versus line-averaged density for one-beam shots (black), two-beam shots (red). These lines are identical to those shown in figure 5(*a*). Also shown are the MAST-Upgrade CS (green triangles) and higher power three-beam simulations representing future upgrades beyond CS (red triangles). One-beam and two-beam shots from previous experiments (blue squares, see [6] for details). Dashed lines: MAST-Upgrade stage 1 with various injection geometries for the nominally on-axis DBB beam with 100 mm $< Z_{\mathrm{RT}} <$ 300 mm (see text for further details). Inset: zoom plot of grey region showing more than a factor of 2 difference in $\partial f/\partial P_{\varphi}$ at density $\sim 4\times10^{19}\,\mathrm{m}^{-3}$ for the extremes of the range of Z_{RT} investigated.

in which flat density profiles can be expected. The flat density profile in these simulations, compared with the peaked density profiles seen in figure 2(*d*), is one of the principal reasons for the low value of $\partial f/\partial\psi_{\mathrm{p,N}}$ for the low-density CS MAST-Upgrade plasma. The possibility of density peaking occurring still exists though, particularly in the low density case in which the beams will fuel the plasma core more efficiently, and in the case of higher density peaking the magnitudes of the term $\partial f/\partial\psi_{\mathrm{p,N}}$ will be larger than those shown.

To mitigate the occurrence of FB modes and consequent FI redistribution in future upgrades beyond CS, it is proposed that the on-axis beam in the DBB be tilted upwards from the horizontal such that the tangency point of its line of sight through the plasma is significantly above the midplane (this vertical distance is referred to as Z_{RT}). The intention is to deposit more fast particles in a moderately off-axis location, contrasting with the core deposition provided by the on-axis beam and the off-axis deposition provided by the off-axis beam. This should result in a FI population which is more evenly distributed over the plasma radius, thus reducing $\partial f/\partial\psi_{\mathrm{p,N}}$ in the FI distribution and the resultant drive for the deleterious FB modes.

A number of simulations were carried out covering a range of inclination angles for the on-axis DBB NB injector, each geometry defined by the height of the tangency point of the line of sight above the midplane (Z_{RT}). The maximum inclination investigated corresponded to $Z_{\mathrm{RT}}=$ 300 mm which results in an inclination of the beamline of 12° upwards from the horizontal. A range of plasma density levels were also investigated from the Greenwald density limit (approximately twice the scenario A1 plasma density) down to the lowest level that could be successfully simulated by TRANSP with this level of injected beam power (about twice the scenario A2 plasma density). For the $Z_{\mathrm{RT}}=$ 300 mm case an additional simulation was executed at the scenario A2 plasma density level with reduced power in the on-axis beam to compare the effect of the DBB modification with the equivalent scenario A2 run (with two off-axis beams at 2.5 MW and one on-axis beam at 1.5 MW, shown as the red triangle at low plasma density in the main plot of figure 8). In each case, the maximum value of $\partial f/\partial\psi_{\mathrm{p,N}}$ has been assessed in the same way as described in section 3.2 using the same radial range for assessment of the uncertainty. It is noted that the maximum values of $\partial f/\partial\psi_{\mathrm{p,N}}$ obtained for the MAST-U simulations were all determined to lie just outside the plasma magnetic axis and in a similar range of pitch-angle space, similar to the analysis of the MAST experimental results in section 3.2.

The dashed lines in figure 8 (main panel) show the results of the MAST-Upgrade simulations including the inclined beam (i.e. one on-axis beam, one off-axis-beam and one tilted-beam with total 7.5 MW injected). At the density levels achievable in the simulations, these cover a relatively small range of $\partial f/\partial\psi_{\mathrm{p,N}}$. For this reason an inset graph has been provided in figure 8, showing a larger scale plot of the grey area in the main plot. Each line represents a different degree of inclination of the beam, identified by the parameter Z_{RT} which runs in 50 mm steps from 100 to 300 mm (the extrema of the scan are labelled in the inset plot). There are two main points to note from this graph. The first point is that the modified geometry of the NBI system leads to lower values of the calculated $\partial f/\partial\psi_{\mathrm{p,N}}$ term. Even without reference to the 'critical' level deduced from the experimental scan in section 3.2, it is clear that mitigation of any FBs in these plasmas is likely to be achieved by implementing the geometry modification. At a plasma density of $\sim 4\times10^{19}\,\mathrm{m}^{-3}$ the difference in $\partial f/\partial\psi_{\mathrm{p,N}}$ more than a factor of 2 between the highest and lowest beam inclination angle. Even if comparing the extents of the uncertainty ranges at this plasma density, the magnitude of the FB mode drive is still reduced by approximately 25%. The extra low density point for the largest beam inclination angle ($Z_{\mathrm{RT}}=300$ mm, plasma density $\sim 1.7\times10^{19}\,\mathrm{m}^{-3}$), when compared with the alternative three-beam geometry simulation indicated by the red triangle at this density level shows that the modified geometry has had a marked effect on the value of $\partial f/\partial\psi_{\mathrm{p,N}}$ reducing it to a level less than the two-beam CS simulation (indicated by the green triangle). The second point to note is that at the largest beam inclination angle investigated, comparison with the experimentally determined 'critical value' indicates that operation over most of this range of plasma densities should avoid FI redistribution by FBs. This conclusion, however, assumes FB resonances in MAST-Upgrade equilibria occur in similar regions of energy and pitch-angle space though uncertainty in the radial location of the possible FB modes has been accounted for, as described earlier.

It is therefore considered that the NBI geometry modification presented in this work is an effective strategy

for mitigation of the effect of FB modes on the FI population. Assessments by the MAST-Upgrade engineering team indicate that tilt angles of the DBB beam close to the maximum proposed here should be achievable without major re-design of the DBB itself. With the proposed modification incorporated into the design, more control over the precise deposition location of beam FIs is made available to the experimentalist, allowing effective heating and current drive as well as control for FI experiments.

5. Conclusions

Results have been presented from eight plasma shots taken on MAST during a recent experimental campaign comprising a systematic four-point scan in plasma density and a simultaneous two-point scan in injected neutral beam power in plasmas designed to be as similar as possible, the only major difference being the plasma electron temperature. Interpretive modelling of these plasmas demonstrates that operation at lower plasma density and/or higher NBI power leads to an increase in the magnitude of the radial gradient of the fast-ion (FI) distribution function, which is taken to be approximately representative of the magnitude of the drive for fishbone (FB) MHD modes. It has further been demonstrated that plasmas with higher absolute magnitude of $\partial f/\partial \psi_{\mathrm{p,N}}$ exhibit higher amplitude $n = 1$ FB modes at similar times in the plasma evolution in which the minimum value of q in the plasma is around 1. Comparison of total neutron emission rate, as measured by a fission chamber, with the predicted neutron emission rate modelled by the TRANSP code shows good agreement in MHD quiescent plasma with an apparent neutron deficit in the measurement in plasmas with larger amplitude FBs. The timing of abrupt drops in the neutron emission rate is well-correlated with the appearance times of the fishbone modes (in agreement with previous studies [5, 6, 30]) so the apparent neutron deficit in the measurement is attributed to redistribution of the FI population by the FBs. It has been demonstrated that the magnitude of the redistribution effect is related to the plasma electron density and the NBI power. The magnitude of the redistribution effect has additionally been shown to be related to the magnitude of the FB mode growth rate which, in turn, is related to the magnitude of the FI distribution function radial gradient through equation (1). Significantly, a region of the parameter space investigated at high plasma density and relatively low beam power has been demonstrated to be free of FI redistribution by FBs either through the complete absence of FBs or due to the low growth rates of FBs, leaving the FI population relatively unperturbed. Identification of this region of the parameter space was the principal intention of the power/density scan which was executed.

Results from the scanning neutron camera have provided a detailed profile of neutron emission in a plasma exhibiting moderate levels of FB activity and FI redistribution effects. Analysis of this profile has provided evidence that the effect of the FBs on the FI population is much larger at a particular position in the plasma core just outboard of the magnetic axis as compared with other radial locations. Similar analysis of the FIDA results produces a result that is consistent with the NC result, confirming that the effect of the FB modes on the FI population is principally localized to the core of the plasma with a weaker effect over a wider radial region. Results obtained using the three diagnostics on MAST sensitive to the FI distribution thus provide a consistent picture of FB-induced FI redistribution in the plasma.

The results obtained during this study have been used in conjunction with detailed modelling of the expected performance of MAST-Upgrade. It has been demonstrated that FI redistribution by FBs should not occur during the Core-Scope stage of MAST-Upgrade at high density, even at full beam power, though FBs and redistribution effects should be expected at lower plasma densities. It has further been shown that the addition of extra NBI power in future upgrades beyond Core Scope may produce moderate to high levels of FI redistribution, with commensurate losses of q-profile control and NB current drive. However a small modification to the geometry of the on-axis DBB beam in future stages of MAST-Upgrade should produce a significant reduction in the magnitude of $\partial f/\partial \psi_{\mathrm{p,N}}$ in the plasma, reducing the drive for MHD and mitigating the subsequent redistribution of the fast ions.

The results presented in this study have been shown to agree qualitatively with the theory of FB stability. Full quantitative analysis will require the coupling of predictive transport codes such as pTRANSP or JINTRAC [33, 34] with an MHD stability code such as MISHKA [27] and a wave–particle interaction code such as HAGIS [29]. Work is ongoing to make such code suites available and it is intended that re-analysis of the plasmas from the present study will be undertaken when the required tools become available.

Acknowledgments

The authors are grateful to Eric Fredrickson for participation in the experiments and subsequent discussions and to Sergei Sharapov and Michael Fitzgerald for discussions concerning FB mode stability. This project has received funding from the European Union's Horizon 2020 research and innovation programme under grant agreement number 633053 and from the RCUK Energy Programme under grant EP/I501045. To obtain further information on the data and models underlying this paper, please contact PublicationsManager@ccfe.ac.uk. The views and opinions expressed herein do not necessarily reflect those of the European Commission.

References

[1] Homfray D.A. *et al* 2011 *Fusion Eng. Des.* **86** 780
[2] Morris A.W. 2012 *IEEE Trans. Plasma Sci.* **40** 682
[3] Milnes J. *et al* 2013 MAST upgrade—progress and engineering challenges *Proc. 25th SOFE (2013)* paper 01-3, pp 1–6
[4] Heidbrink W.W. and Sadler G.J. 1994 *Nucl. Fusion* **34** 535
[5] Johnson D. *et al* 1983 *Proc. 9th Int. Conf. on Plasma Physics and Controlled Nuclear Fusion Research (Baltimore, MD, 1982)* vol 1 (Vienna: IAEA) p 9
[6] Turnyanskiy M. *et al* 2013 *Nucl. Fusion* **53** 053016
[7] Stammers K. 2006 *Nucl. Instrum. Methods Phys. Res.* A **562** 521
[8] Cecconello M. *et al* 2014 *Nucl. Instrum. Methods* A **753** 72
[9] Michael C.A. *et al* 2013 *Plasma Phys. Control. Fusion* **55** 095007

[10] Walsh M.J. *et al* 2003 *Rev. Sci. Instrum.* **74** 1663
[11] Tournianski M.R. *et al* 2001 *Nucl. Fusion* **41** 77
[12] Tournianski M.R. *et al* 2003 *Rev. Sci. Instrum.* **74** 2089
[13] Patel A. *et al* 2004 *Rev. Sci. Instrum.* **75** 4944
[14] De Bock M.F. *et al* 2008 *Rev. Sci. Instrum.* **79** 10F524
[15] Lao L.L. *et al* 1985 *Nucl. Fusion* **25** 1611
[16] Goldston R.J. *et al* 1981 *J. Comput. Phys.* **43** 61
[17] Pankin A. *et al* 2004 *Comput. Phys. Commun.* **159** 151–84
[18] Stirling W.L. *et al* 1979 *Rev. Sci. Instrum.* **50** 102
[19] Duesing G. *et al* 1987 *Fusion Technol.* **11** 163
[20] Cecconello M. and Klimek I., private communication
[21] Chen L. *et al* 1984 *Phys. Rev. Lett.* **52** 1122
[22] Heidbrink W.W. 2008 *Phys. Plasmas* **15** 055501
[23] Mikkelsen D.R. 1989 *Nucl. Fusion* **29** 1113
[24] Klimek I. *et al* 2015 TRANSP modelling of neutron emissivity profiles measured by a neutron flux monitor *Nucl. Fusion* submitted
[25] Wodniak I. *et al* 2012 *39th EPS Conf. on Plasma Physics (Stockholm, Sweden, 2–6 July 2012)* P5.077
[26] Cecconello M. *et al* 2015 *Plasma Phys. Control. Fusion* submitted
[27] Mihailovskii A.B. *et al* 1997 *Plasma Phys. Rep.* **23** 844
[28] Jones O.M. *et al* 2013 *Plasma Phys. Control. Fusion* **55** 085009
[29] Pinches S.D. *et al* 1998 *Comput. Phys. Commun.* **111** 133
[30] Perez von Thun C. *et al* 2010 *Nucl. Fusion* **50** 084009
[31] Keeling D.L. 2008 *International Spherical Tori Workshop (Madison, WI, 2009)*
[32] ITER Physics Basis 1999 *Nucl. Fusion* **39** 2137
[33] http://w3.pppl.gov/transp/
[34] Cherubini A. *et al* 1996 *Plasma Phys. Control. Fusion* **38** 1421